HHS Public Access

Author manuscript

*Dev Cell*. Author manuscript; available in PMC 2021 June 08.

Published in final edited form as:

*Dev Cell*. 2020 June 08; 53(5): 503–513.e5. doi:10.1016/j.devcel.2020.04.012.

# *Snai2* maintains bone marrow niche cells by repressing osteopontin expression

**Qiaozhi Wei**[1,2], **Fumio Nakahara**[1,2,*], **Noboru Asada**[1,2,#], **Dachuan Zhang**[1,2], **Xin Gao**[1,2], **Chunliang Xu**[1,2], **Alan Alfieri**[3], **N. Patrik Brodin**[3], **Samuel E. Zimmerman**[4,5], **Jessica C. Mar**[4,5], **Chandan Guha**[3,6,7], **Wenjun Guo**[1,2], **Paul S. Frenette**[1,2,3,8,$]

[1]Ruth L. and David S. Gottesman Institute for Stem Cell and Regenerative Medicine Research, Albert Einstein College of Medicine, Bronx, New York 10461, USA.

[2]Department of Cell Biology, Albert Einstein College of Medicine, Bronx, New York 10461, USA.

[3]Department of Radiation Oncology, Albert Einstein College of Medicine, Bronx, New York 10461, USA.

[4]Department of Systems and Computational Biology, Albert Einstein College of Medicine, Bronx, New York 10461, USA.

[5]Department of Epidemiology and Population Health, Albert Einstein College of Medicine, Bronx, New York 10461, USA.

[6]Department of Pathology, Albert Einstein College of Medicine, Bronx, New York 10461, USA.

[7]Department of Urology, Albert Einstein College of Medicine, Bronx, New York 10461, USA.

[8]Department of Medicine, Albert Einstein College of Medicine, Bronx, New York 10461, USA.

## Summary

Bone marrow (BM) mesenchymal stem and progenitor cells (MSPCs) are a critical constituent of the hematopoietic stem cell (HSC) niche. Previous studies have suggested that the zinc-finger epithelial-mesenchymal transition transcription factor *Snai2* (also known as *Slug*) regulated HSCs autonomously. Here, we show that *Snai2* expression in the BM is restricted to the BM stromal

**Correspondence:** Paul S. Frenette, Albert Einstein College of Medicine, Michael F. Price Center, 1301 Morris Park Avenue, Room 101, Bronx, NY 10461, paul.frenette@einsteinmed.org, Tel: 718.678.1255, Fax: 718.678.1018.

*Faculty of Medicine, The University of Tokyo, Tokyo, Japan;

#Department of Hematology, Oncology and Respiratory Medicine, Okayama University, Okayama, Japan.

$Lead Contact.

Author Contributions

Q.W. performed most of experiments, analyzed data and wrote the manuscript. F.N. contributed to multiple *in vitro* assays and preliminary studies. N.A. helped analyzing the *Snai2*$^{YFP}$; *Ng2*-Cre; *R26*-tdTomato mice. D.Z. and X.G. helped with mouse treatments and analysis. C.X. helped with MSPC differentiation assays. A.A., N.P.B. and C.G. performed the targeted limb irradiation. S. Z. and J.M. helped with RNA-seq analysis. W.G. contributed to the experimental design and manuscript. P.S.F. supervised the study and wrote the manuscript. All authors discussed the results and contributed to the manuscript.



Declaration of Interests

P.S.F. has served as consultant for Pfizer, received research funding from Ironwood Pharmaceuticals and owns stock options of Cygnal Therapeutics.

compartment where it regulates the HSC niche. Germline or MSPC-selective *Snai2* deletion reduces the functional MSPC pool, their mesenchymal lineage output, and impairs HSC niche function during homeostasis and after stress. RNA-sequencing analysis revealed that *Spp1* (osteopontin) expression is markedly upregulated in *Snai2*-deficient MSPCs. Genetic deletion of *Spp1* in *Snai2*-deficient mice, rescues MSPCs' functions. Thus, SNAI2 is a critical regulator of the transcriptional network maintaining MSPCs by the suppression of osteopontin expression.

## eTOC Blurb

Wei et al found that *Snai2* is preferentially expressed and required in bone marrow mesenchymal stem and progenitor cells (MSPC) for their maintenance and regeneration. The authors show that *Snai2* promotes self-renewal by suppressing *Spp1* expression in MSPCs.

### Keywords

Bone marrow; mesenchymal stem and progenitor cells; stromal cells; *Snai2/Slug*; osteopontin (OPN)/Spp1; self-renewal; hematopoietic stem cell niche; transcriptional regulation

## Introduction

Bone marrow (BM) mesenchymal stem cells (MSPCs) comprise self-renewing and multipotent precursor cells that can give rise to bone, cartilage, fat and hematopoiesis-supporting marrow stroma (Bianco et al., 2013; Frenette et al., 2013). Their critical roles in supporting hematopoiesis and, in particular, hematopoietic stem cells (HSCs) have increasingly been recognized over the past two decades. During development, MSPCs were reported to associate with hematopoietic sites (Mendes et al., 2005). In adult animals, MSPCs are a major provider of the essential niche factors (e.g. SCF, CXCL12, Pleiotrophin and IL-7) for HSC maintenance and progenitor differentiation (Cordeiro Gomes et al., 2016; Ding and Morrison, 2013; Ding et al., 2012; Greenbaum et al., 2013; Himburg et al., 2018; Mendez-Ferrer et al., 2010). However, despite these critical functions, the mechanisms regulating MSPC maintenance in the bone marrow remain largely unknown.

Transcription factors are critical cell fate determinants. A few transcription factors have been suggested to regulate BM development or HSC niche (Kieslinger et al., 2010; Liu et al., 2018; Omatsu et al., 2014; Seike et al., 2018), yet the network of factors that specify MSPC and maintain BM homeostasis have not been elucidated. The challenge is in part due to the poorly defined organization of the heterogeneity and differentiation hierarchy within the mesenchymal lineage (Baryawno et al., 2019; Severe et al., 2019; Tikhonova et al., 2019). A transcription regulatory network specific to MSPCs and their progeny will be needed to understand the BM niche maintenance and function.

Our transcriptomic analyses of MSPCs have revealed that *Snai2* (also known as *Slug*), an epithelial-mesenchymal transition (EMT) transcription factor, was highly expressed in BM *Nes*-GFP$^{+}$ niche cells (Kunisaki et al., 2013; Nakahara et al., 2019). EMT transcription factors have been associated with mesenchymal traits and stem cell characteristics during healthy developmental and pathogenic malignant programs (Guo et al., 2012; Mani et al.,

2008; Medici et al., 2010), raising the possibility that *Snai2* may regulate MSPCs in the BM niche.

## Results

### *Snai2* is selectively expressed in BM MSPCs

Our transcriptome analysis of *Nes*-GFP$^+$ BM MSPCs (Kunisaki et al., 2013) revealed high expression levels of EMT transcription factors, among which, *Snai2*, a *Snail* family zinc finger protein, showed the highest transcript levels (Figure 1A). Two independent transcriptome profilings (Cabezas-Wallscheid et al., 2014; Maryanovich et al., 2018) found negligible *Snai2* expression in HSCs. To map precisely *Snai2* expression within the BM, we crossed *Snai2*$^{YFP}$ reporter mice, in which the yellow fluorescent protein (YFP) driven by an internal ribosome entry site (IRES) was targeted into the 3'UTR of the *Snai2* locus (Guo et al., 2012), with *Ng2*-Cre; *R26*-tdTomato double transgenic mice in which the Tomato expression labels *Nes*-GFP$^+$ niche cells (Asada et al., 2017). Both imaging and flow cytometry analyses revealed that *Snai2*$^{YFP}$ expression labeled virtually all (~97%) the NG2-marked BM mesenchymal cells, including the peri-arteriolar, sinusoidal and interstitial stromal cells (Figure 1B and C), while rare single positive cells may reflect heterogeneity of the BM stroma or the dynamic expression of the reporter transgenes. Similar results were obtained in the *Snai2*$^{YFP}$; *Lepr*-Cre; *R26*-tdTomato mice consistent with the largely overlapping expression of these two Cre lines in the non-arteriolar stromal cells (Asada et al., 2017; Ding et al., 2012) (Figure S1A and B). Furthermore, *Snai2*$^{YFP}$ expression was absent in endosteal osteoblasts (Figure 1B and Figure S1A and C), suggesting that *Snai2* was specifically expressed in the mesenchymal stem and progenitor fraction but not in their differentiated progeny. Additionally, our analysis of the *Snai2*$^{YFP}$ reporter and endogenous *Snai2* transcript in sorted BM populations only detected *Snai2* expression in the mesenchymal cell fractions but not in hematopoietic cells, including purified HSCs and progenitors (Figure 1D–G). *Snai2*$^{YFP+}$ cells were enriched in niche factor expression and fibroblastic colony forming activity (CFU-F) in BM, further confirming *Snai2* expression in the MSPC compartment (Figure 1H and I).

### *Snai2* deletion reduces bone marrow MSPC numbers

To investigate *Snai2*'s function, we first analyzed BM MSPCs in previously described *Snai2*-deficient (*Snai2*$^{LacZ}$, hence as *Snai2*$^{-/-}$) mice (Jiang et al., 1998), bred with *Nes*-GFP transgenic mice to label MSPCs (Mendez-Ferrer et al., 2010). As these mice do not survive into adulthood on a pure C57/BL6 background, we intercrossed *Snai2*$^{+/-}$ with 129Sv wild-type mice to obtain 129Sv/C57BL/6 F1 generation and hence *Snai2*$^{-/-}$ and littermate control animals. At 8 weeks of age, *Snai2*$^{-/-}$ BM showed a mild reduction of cellularity compared to wild-type littermates (Figure 2A), and a reduced frequency and absolute number of CD45$^-$ Ter119$^-$ CD31$^-$ CD51$^+$ PDGFRα$^+$ MSPCs (Pinho et al., 2013) or *Nes*-GFP$^+$ cells (Figure 2B–D). Furthermore, sorted *Snai2*$^{-/-}$ MSPCs formed significantly fewer and smaller mesenspheres (Figure 2E–G) and CFU-F colonies (Figure S1D and E), which indicate an impaired self-renewal capacity. Immunofluorescence examination of *Snai2*$^{-/-}$ bones revealed a reduced lining of the trabeculae by mature osteoblasts marked by osteocalcin, a noncollagenous secreted protein produced exclusively by osteoblasts (Figure 2H). We also

observed an absence of adipocytes marked by BODIPY, a lipid droplet tracing dye, and Perilipin, the major lipid droplet coating protein (Figure 2I), consistent with the reported absence of white adipose tissues in *Snai2*$^{-/-}$ mice (Perez-Mancera et al., 2007). To investigate further if the reduced adipocytes originated from an MSPC defect, we challenged control and *Snai2*$^{-/-}$ mice with 6 Gy irradiation, an injury shown to induce adipogenesis from BM MSPCs *in vivo* (Mizoguchi et al., 2014). We found that *Snai2*$^{-/-}$ MSPCs differentiation into Perilipin$^{+}$ adipocyte was markedly reduced (Figure S1F). In addition, micro-CT analysis of *Snai2*$^{-/-}$ femurs revealed that the bone formation was impaired as shown by significantly reduced mineralized trabecular and cortical bone volumes (Figure 2J, K). These data suggest that *Snai2* deletion impairs the self-renewal capacity and multi-lineage output of BM MSPCs.

### *Snai2* deletion alters the HSC niche both at steady state and after stress

We next asked if the MSPC defects produced by *Snai2* deletion resulted in alterations of hematopoiesis. *Snai2*$^{-/-}$ mice presented a mild anemia and a slight increase in white blood cell counts and platelet numbers in blood (Figure S1G). The frequency and absolute number of Lineage$^{-}$ Sca1$^{+}$ ckit$^{+}$ CD150$^{+}$ CD48$^{-}$ HSCs (Figure 3A) and CD45$^{-}$ CD11b$^{-}$ CD71$^{+}$ Ter119$^{+}$ erythroblasts (Figure S2A) were significantly reduced in *Snai2*$^{-/-}$ BM compared to controls. Cell cycle analysis indicated that higher proportion of HSCs resided in the G0 phase in *Snai2*$^{-/-}$ BM compared to controls (Figure 3B), suggesting increased quiescence.

Previous studies have reported that *Snai2*-null mice die from total body irradiation at a dose that wild-type control mice could survive and attributed it to hematopoietic cell-intrinsic defects (Inoue et al., 2002; Perez-Losada et al., 2003; Wu et al., 2005). By contrast, we have found that wild-type BM donor cells could not rescue lethally irradiated *Snai2*$^{-/-}$ recipients and anemia was observed in the dying *Snai2*$^{-/-}$ recipient animals (Figure S2C–E), suggesting a defective BM microenvironment during recovery. This defect was not due to impaired homing of donor cells into the *Snai2*$^{-/-}$ BM as the number of migrated hematopoietic cells in lethally irradiated mutant and wild-type mice was similar (Figure S2F). Similarly, most *Snai2*$^{-/-}$ mice died after a single dose of 250 mg/kg 5-flurouracil (5FU) challenge while all wild-type littermates survived (Figure S2G). We found no significant difference in rates of MSPC apoptosis (Figure S2H) one day after 5FU. Moreover, in radiation chimeras in which the recipients are wild type, *Snai2*$^{-/-}$ BM cells did not show any deficit in recovery after 5FU (Figure S2I). These functional results, combined with the expression data, clearly indicate that SNAI2 is acting on the non-hematopoietic compartment and is critical in the recovery after genotoxic insults.

We then surmised that the impaired MSPC niche in *Snai2*$^{-/-}$ BM led to reduced HSC self-renewal and retarded BM recovery after myeloablation. We evaluated HSC distributions relative to various quiescence-regulating niches in the *Snai2*$^{-/-}$ BM by confocal immunofluorescence imaging (Bruns et al., 2014; Kunisaki et al., 2013; Pinho et al., 2018; Zhao et al., 2014; Zhao et al., 2019), and found significantly closer association of HSCs with *Nes*-GFP$^{high}$ MSPC-associated arterioles, but not with megakaryocytes or bones (Figure 3C and S2J and K). Interestingly, we observed a disproportional loss of *Nes*-GFP$^{low}$ sinusoidal and interstitial MSPCs but not the *Nes*-GFP$^{hi}$ MSPCs in the *Snai2*$^{-/-}$ BM (Figure 3D and

S2L). This also suggests that *Snai2* is required in *Nes*-GFP$^{low}$ mesenchymal niche cells but not in the hematopoietic or bone-associated stromal populations (Figure 1B and Figure S1A and C). To further exclude the possibility that hematopoiesis might be affected indirectly by *Snai2* expression outside of BM, we carried out targeted irradiation studies in which we irradiated one limb of the control or *Snai2*$^{-/-}$ mice using CT-guided X-ray such that only a small localized fraction of the total bone marrow was ablated (Figure 3E). One week after targeted irradiation, control or *Snai2*$^{-/-}$ mice showed similar numbers of live hematopoietic and stromal cells. However, at two weeks post-irradiation, the irradiated limbs from wild-type mice showed full recovery in cellularity (~120% of the non-irradiated limb) whereas *Snai2*$^{-/-}$ limbs exhibited significantly lower cellularity (~75% of the non-irradiated side; Figure 3F). The HSC and LSK numbers of the control limbs also recovered to non-irradiated levels at two weeks while their recovery in *Snai2*$^{-/-}$ limbs remained significantly impaired (Figure 3G). This was associated with a severe reduction of the MSPCs and endothelial cells in the irradiated *Snai2*$^{-/-}$ limbs (Figure 3H). Therefore, our results indicate that the recovery defects of *Snai2*$^{-/-}$ animals are not due to the impaired cell survival after stress, but rather to a compromised recovery of niche cells.

## Gene expression changes in *Snai2*-deficient MSPCs

To gain mechanistic insights on *Snai2*-mediated regulation of BM MSPC activity, we conducted a transcriptome analysis on sorted control and *Snai2*$^{-/-}$ BM MSPCs. We detected 154 significantly up-regulated and 85 down-regulated ($p$ value<0.05, counts per million>20, fold change>2) genes in *Snai2*$^{-/-}$ MSPCs compared with controls. Ingenuity Canonical Pathway analysis revealed that the most differentially expressed genes were enriched in extracellular matrix (ECM) signaling and remodeling, fibrosis and integrin signaling (Table S1–S2). An unbiased Gene Set Enrichment Analysis (GSEA) also identified a significant up-regulation of genes in ECM-receptor interaction in *Snai2*$^{-/-}$ MSPCs (Figure S3A). GSEA further revealed that genes involved in osteogenesis and chondrogenesis were highly up-regulated (Figure S3B) while adipogenesis was not significantly changed (Figure S3C), suggesting an altered mesenchymal differentiation program. By contrast, genes encoding HSC niche factors, such as *Cxcl12*, *Kitl*, *Angpt1*, *Vcam1*, and *Il7*,, were minimally affected by *Snai2* deletion with the exception of *Spp1*(osteopontin) which was highly up-regulated and confirmed by RT-PCR (Figure 4A and B and S3D). *Snai2* was reported to antagonize the p53-mediated apoptosis pathway in other cell types (Kurrey et al., 2009; Wu et al., 2005). Although we detected a significant up-regulation of p53 targets (Kannan et al., 2001) in *Snai2*$^{-/-}$ MSPCs, a reported SNAI2 targets involved in DNA damage response, Puma (encoded by *Bbc3*) (Wu et al., 2005), was unchanged (Figure S3E and F). *Cdkn1a*, encoding the cyclin-dependent kinase inhibitor p21Waf1/Cip1 and a known SNAI2 target (Chen and Gridley, 2013), was significantly up-regulated (Figure S3F) while the expression of *Foxc1*, a critical transcription regulator of MSPC differentiation (Omatsu et al., 2014), was unchanged (Figure S3D).

## *Snai2* regulates adult BM MSPCs via suppression of osteopontin

Based on these results, we focused on *Spp1* (osteopontin or OPN) as a candidate downstream effector of *Snai2* in BM niche regulation. Previous studies have suggested that *Snai2* directly binds to the *Spp1* promoter (Kurrey et al., 2009). OPN is an extracellular

matrix glycoprotein previously suggested to be a negative regulator of BM HSC number and ageing (Guidi et al., 2017; Nilsson et al., 2005; Stier et al., 2005). Although it is highly enriched in the endosteum (McKee et al., 1993), *Spp1* transcript is mostly expressed by subsets of mesenchymal stromal cells that are found throughout the BM (Tikhonova et al., 2019). In addition, MSPCs express receptors (integrins and CD44) for OPN (Denhardt et al., 2001) (Figure S3G), enabling a potential autocrine signaling. Yet, the role of OPN in MSPC activity is unclear. We thus reasoned *Snai2* might regulate MSPC self-renewal and HSC number via *Spp1* suppression. To test this hypothesis, we cultured wild-type BM MSPCs at clonal density in the presence of an OPN-blocking antibody (Kiefer et al., 2010). We found that OPN blockade markedly increased the ability to form mesenspheres compared to the IgG control group (Figure 4C), suggesting that extracellular OPN may play an autocrine inhibitory role in MSPC self-renewal.

To overcome the lethality of *Snai2* deletion in the germline, we generated a floxed allele of *Snai2* (*Snai2*$^{floxed}$) using CRISPR/Cas9 technology (Figure S3H) and crossed it with *Mx1*-Cre (*Snai2*$^{floxed/floxed}$; *Mx1*-Cre, hereafter as *Snai2*$^{Mx1\text{-}Cre}$) to knockout *Snai2* postnatally (Figure 4D). Polyinosine-polycytidylic acid (pIpC) injections induced efficient deletion of *Snai2* in adult BM MSPCs of *Snai2*$^{Mx1\text{-}Cre}$ mice as previously described (Figure 4E) (Park et al., 2012). Consistent with *Snai2*$^{-/-}$ mice, postnatal *Snai2* deletion resulted in significant reductions of BM MSPC numbers, mesensphere-forming capacity, up-regulation of *Spp1* mRNA and reduction in BM HSC numbers (Figure 4E–H), while BM cellularity and MSPC niche factor expression were not affected (Figure S4A–C). These results confirmed that *Snai2* is required for not just the development of BM MSPCs but also their maintenance during homeostasis. We then crossed *Snai2*$^{Mx1\text{-}Cre}$ mice with *Spp1* knockout (*Spp1*$^{-/-}$) animals to evaluate the impact of OPN on the phenotype of *Snai2*-deficient mice. We found that in the absence of OPN, MSPC numbers and sphere-forming capacity were rescued and *Cdkn1a* upregulation after *Mx1*-Cre-induced *Snai2* deletion was also reversed (Figure 4E–G and S4D), clearly indicating that *Snai2* suppression of *Spp1* expression is critical for BM MSPC self-renewal and maintenance. Interestingly, BM HSC numbers were reduced in *Snai2* conditional knockout mice (CKO) regardless of *Spp1* expression (Figure 4H), suggesting that other factors might contribute to the reduced HSC niche function of *Snai2*-deficient MSPCs.

To further examine the role of *Snai2* and *Spp1* in BM regeneration and exclude the potential contribution of *Snai2* expression in hematopoietic cells, we subjected the pIpC-induced *Snai2*$^{Mx1\text{-}Cre}$; *Spp1*$^{-/-}$ mice to lethal irradiation and reciprocal BM transplantation using CD45.1 wild-type donor cells (Figure 4I). *Snai2*$^{Mx1\text{-}Cre}$ CKO mice were viable after reciprocal BM transplant and their BM cellularity were able to recover to near the wild-type levels (Figure S4E–G). However, the BM MSPC numbers were significantly reduced in *Snai2* CKO (Figure S4G), despite a complete replacement of their BM by wild-type hematopoietic cells. Reciprocally transplanted *Snai2* CKO mice also displayed reduced HSC numbers (CD45.1) in their BM (Figure S4H), which was confirmed by reduced repopulation in secondary competitive BM transplantation (Figure S4I). Analysis of the CKO MSPCs revealed unchanged niche factor but up-regulated *Spp1* and *Cdkn1a* mRNA expression (Figure S4J), consistent with our observations in *Snai2*$^{-/-}$ mice. Importantly, the reduction in HSC repopulation activity was due to *Snai2* deletion in niche cells—not HSCs— because

when HSCs were sorted from *Snai2*CKO BM, they performed slightly better than those from control mice (Figure S4K), consistent with their more quiescent cell cycle profile (Figure 3B). Intriguingly, *Snai2*$^{Mx1\text{-}Cre}$; *Spp1*$^{-/-}$ mice displayed wild-type levels of BM MSPC (Figure 4I), indicating that *Snai2*-mediated *Spp1* suppression in MSPCs is critical for BM recovery. In addition, reduced HSC number in *Snai2*$^{Mx1\text{-}Cre}$ mice was also restored upon *Spp1* deletion, as shown by both phenotypic FACS analysis (Figure 4I), secondary competitive BM transplantation (Figure 4J), and normalized repopulation activity from isolated HSCs (Figure S4K). Altogether, our results indicate that *Snai2* regulates BM MSPC and HSC activities via suppression of *Spp1* in BM MSPCs.

## Discussion

The molecular basis of BM MSPCs' maintenance and multi-lineage potency remains poorly understood. MSPCs originate at least in part from the neural crest (Isern et al., 2014; Morikawa et al., 2009), a developmental cell population that gives rise to diverse lineages including peripheral neurons, muscle and bone. The formation of neural crest involves the EMT process (Kalcheim, 2015), and studies in lower vertebrates have implicated a critical role of the EMT transcription factor *Snai2* in the formation of these neural-crest derivatives (Mancilla and Mayor, 1996; Nieto et al., 1994). Although *Snai2* is also expressed in migratory neural crest cells of mouse embryos, it is not required for the formation of these cells (Jiang et al., 1998), indicating an evolutionarily distinct functions. Here, our results indicate that *Snai2*, is essential for maintaining the functional pool of MSPCs in adult BM. Deletion of *Snai2* results in reduced MSPC numbers and impaired MSPC self-renewal and lineage output. This is associated with an altered lineage differentiation gene signature, up-regulation of p53 target genes and fibrosis-related genes. Thus, *Snai2* represents a master regulator of MSPC's multipotent state in part by suppressing aberrant differentiation or senescence program.

MSPCs can gain the capacity to induce a hematopoiesis-supporting marrow and maintain definitive HSCs. The present data raise the possibility that *Snai2* may take part of the regulatory network ensuring HSC niche function and this activity is not mediated via the modulation of the niche factor CXCL12 or SCF. It is notable that *Snai2* deletion resulted in a preferential loss of *Nes*-GFP$^{Lo}$, ubiquitously distributed, peri-sinusoidal MSPCs, but relative enrichment of *Nes*-GFP$^{Hi}$ peri-arteriolar niche cells. This may explain the alterations in HSC quiescence status since the peri-arteriolar niche contribute to maintaining HSC quiescence (Asada et al., 2017; Kunisaki et al., 2013; Pinho et al., 2018).

Our results have uncovered an autocrine function of OPN in MSPC regulation and *Snai2* regulates the BM MSPC pool size at least in part via suppression of OPN. OPN is one of the most abundantly deposited glycoprotein in the BM extracellular matrix and a negative regulator of BM HSPC pool size via microenvironment-mediated mechanisms that have not been clearly defined (Nilsson et al., 2005; Stier et al., 2005). It is intriguing that MSPCs are a major producer of OPN in the BM based on mRNA abundance and they express receptors for OPN as well. Our results suggest that, in addition to a direct restrictive role on HSC expansion, OPN might also restrict HSC numbers by restricting BM MSPC numbers. Our findings also indicate that OPN's autocrine inhibitory role on MSPC self-renewal may be a

potential mechanism by which BM MSPCs sense the need from the BM microenvironment to regenerate. In summary, our study identifies a *Snai2-Spp1* axis regulating BM MSPC self-renewal and HSC niche function.

# STAR METHODS

## RESOURCE AVAILABILITY

**Lead Contact—**Further information and requests for resources and reagents should be directed to and will be fulfilled by: Paul S. Frenette (paul.frenette@einsteinmed.org).

**Materials Availability—**This study has generated a *Snai2*$^{floxed}$ mouse line, which can be made available upon request and requires a Material Transfer Agreement (MTA).

**Data and Code Availability—**Raw and processed reads data from the RNA-seq have been deposited in the Gene Expression Omnibus under accession number GSE142705.

## EXPERIMENTAL MODEL AND SUBJECT DETAILS

**Mice—***Snai2*$^{-/-}$, previously as *Slug*$^{LacZ}$, (Jiang et al., 1998) and *Snai2*$^{YFP}$ knockin (Guo et al., 2012) mice are previously described. *Snai2*$^{floxed}$ mice were generated at the Gene Modification Facility of Albert Einstein College of Medicine as described below. C57BL/6 (CD45.2) and Bl6-Ly5.1 (CD45.1) mice were purchased from Charles River Laboratories (Frederick Cancer Research Center, Frederick, MD)/NCI or the Jackson Laboratories (B6.SJL-*Ptprc*$^{a}$ *Pepc*$^{b}$/BoyJ). *Ng2*-Cre (B6; FVB-Tg(Cspg4-cre)1Akik/J), *Lepr*-Cre (B6.129-Leprtm2(cre)Rck/J), *R26*-tdTomato (B6.Cg-*Gt(ROSA)26Sortm14(CAG-tdTomato)Hze*/J), *Mx1*-Cre (B6.Cg-Tg(Mx1-cre)1Cgn/J) and *Spp1*$^{-/-}$ (Spp1Tm1Blh/J) mice were from Jackson Laboratories. All animals were housed in specific pathogen-free barrier facility and all experimental procedures were approved by the Animal Care and Use Committee of Albert Einstein College of Medicine. All experiments or start of treatments were performed on mice of both genders with littermate controls from the same colony between 8–16 weeks of age.

**Generation of *Snai2*$^{floxed}$ mice by CRISPR/Cas9—**Two loxp sites were inserted into the endogenous *Snai2* locus sequentially by CRISPR/Cas9 technology. gRNAs targeting to intron 1 (gRNA1: ggagattgctgctcaggcga ggg) and Exon 3 un-translated region (gRNA2: ttactgacagctagattgaa agg) of mouse *Snai2* gene respectively were designed by an online tool (http://crispr.mit.edu/) and generated by in vitro transcription (Yang et al., 2013). Cas9 mRNA was purchased from SBI. The single-stranded *Snai2* conditional knockout homologous recombination donor (HRDs) carrying 60nt homologous arms at each side and surrounded loxp sites (HRD1: ttctctgagcctgtgtgtacgcaaaaggagtgcacggacgtgatcgcacccttcccctcg TCTGATAACTTCGTATAATGTATGCTATACGAAGTTATtgagcagcaatctcctgaagccaagcactt gggaaagcagctggattcgtgcatgccatt, HRD2: gtacttaaagttaattcgttctatgtgaagtttaaaattatatttactgacagctagattATAACTTCGTATAATGTATGCT ATACGAAGTTATcgataccgtcgacctcggaaaggataaagataagaat ctttctctttaaagatgaagtgaaaagcacattgcatct) were synthesized from IDT. C57BL6 female mice

(3–4 weeks old) were super-ovulated by intra-peritoneal PMS (5 IU/mouse day1) and HCG (5 IU/mouse day 3) injections and mated to C57BL6 males. Fertilized embryos were collected from oviducts. The gRNAs, Cas9 mRNA and *Snai2* conditional knockout HRDs were mixed and microinjected into the cytoplasm of fertilized eggs. The injected zygotes were transferred into pseudopregnant CD1 females, and the resulting pups were obtained and genotyped by sequencing PCR clones from the targeted region. Mice successfully inserted 3' loxp site were obtained first and expanded as donors for 5' loxp insertion. Mice successfully incorporated both loxp sites were bred to C57BL6 mice to remove potential off-targets and establish the *Snai2*$^{floxed}$ colony. The top ten predicted off-target sites were examined by targeted sequencing. A null allele of *Snai2* was also generated as a by-product of the gRNA injections. Once established, the *Snai2*$^{floxed}$ allele was genotyped by ear clip genomic DNA PCR using primers: *Snai2* 5'GTF: tgagatctttgctgacaaggaa and *Snai2* 5'GTR: ctagctgtaccgtgcctgtg (WT: 196bp, *Snai2*$^{floxed}$: 233bp). *Snai2* Rev_3: tgatgacaaccaggcatcat and *Snai2* FOR_6: tgacaaatgaaagtccaaagaca (WT: 500bp, *Snai2*$^{floxed}$: 550bp).

**Primary cell culture—**For CFU-F assays, 1–3×$10^3$ sorted *Nes*-GFP$^+$ or CD45$^-$ Ter119$^-$ CD31$^-$ CD51$^+$PDGFRα$^+$ MSPCs were seeded per well in a 6-well adherent tissue culture plate using phenol-red freeα-MEM (Gibco) supplemented with 20% FBS (Hyclone), 10% MesenCult stimulatory supplement (Stem Cell Technologies) and 0.5% penicillin-streptomycin. One-half of the media was replaced after 7 days and at day 14 colonies were stained with Giemsa staining solution (EMD Chemicals) and numerated under a bright field microscope. For mesensphere assays, MSPCs were plated in sphere media (15% chicken embryo extract, 0.1mM 2-Mercaptoethanol, 1% non-essential amino acids, 1% Pen-Strep, 1% N2 and 2% B27 supplements (Gibco) in 1:2 DMEM/F12: human endothelial-SFM, filter-sterilized and supplemented with 20 ng/ml fibroblast growth factor (FGF)-basic, insulin-like growth factor-1 (IGF-1), epidermal growth factor (EGF), platelet-derived growth factor (PDGF) and oncostatin M (OSM) (Peprotech) at clonal density (<500 cells/cm$^2$) in ultralow adherent-culture dishes (Stem Cell Technology) as previously described (Pinho et al., 2013). Once plated, cells were kept at 37°C 5% CO2 in a water jacketed incubator untouched for 1 week to prevent cell aggregation. Half media change was performed at 1 week and spheres with >4 cells were numerated at day 9. For testing the relevance of OPN in mesensphere formation, MSPCs were sorted at 500 /well into 96-well ultralow attachment plates (Corning #3474) in sphere media supplemented with 10 μg/ml anti-OPN (R&D#: AF808) or goat IgG.

## METHOD DETAILS

**Flow cytometry and cell sorting—**Bone marrow stromal cells were isolated as described previously with minor modifications (Kunisaki et al., 2013). Briefly, bone marrow plugs were flushed out by inserting a 21G needle attached to a 1 ml syringe filled with digestion buffer (1 mg/ml Collagenase IV, 2 mg/ml Dispase and 1 mg/ml DNase I in PBS) and then incubated for ~30 min in the digestion buffer with gentle rocking at 37°C. Single cell suspension was then generated by gently inverting the tubes. When stromal components are not required for analysis, femurs were flushed gently with 1 ml of ice-cold PEB (PBS/2 mM EDTA / 0.5% BSA) buffer using a 1 ml syringe (BD) into single cell suspension by passing through a 21G needle (BD) into FACS tubes. The single cell suspension was then

pelleted, and RBCs lysed by an ammonium chloride solution. The resulted BM nucleated cells (BMNCs) were then identified and counted as trypan blue excluding cells under the microscope. When analyzing erythroblasts, the BM was processed as described before (Wei et al., 2019). About $2\times10^6$ BMNCs were then processed for each FACS staining. Stained sample suspensions were acquired on an LSR II flow cytometer. DAPI-negative singlets were analyzed for all live samples unless otherwise specified. For sorting, samples were processed under sterile conditions and sorted on a FACSAria II (BD). Data were analyzed using FACS Diva (BD) or FlowJo (Tree Star) software.

**Complete blood count—**Mice were bled ~25 μl into an Eppendorf tube containing 2 μl of 0.5 M EDTA (Life Technologies) using heparinised micro-haematocrit capillary tubes (Fisherbrand) under isoflurane anaesthesia. Blood was diluted 1:20 in PBS and analysed on an Advia counter (Siemens).

**Immunofluorescence imaging—**Whole-mount sternum HSC immunofluorescence staining and imaging analysis were performed as previously described (Bruns et al., 2014; Kunisaki et al., 2013; Pinho et al., 2018). Briefly, Alexa Fluor 647-anti-VE-Cadherin (BV13) (Biolegend) and APC-anti-CD31/PECAM-1 (MEC13.3) were infused 10 min before sacrificing the mice to label vasculature *in vivo*. Sternum segments were then harvested, cleaned and bisected sagittally with a surgical blade into individual halves to expose the marrow cavity. Fragments were re-fixed with 4% PFA; blocked and permeabilized in PBS with 10% normal goat serum and 0.5% Triton X-100 and stained with primary antibodies (biotin anti-Lineage panel cocktail, biotin anti-CD48 and PE anti-CD150) for 3 days. After three PBS washes, the tissues were then incubated with streptavidin eFluor 450 for 2 h. Images were acquired on a ZEISS Axio examiner D1 microscope with a confocal scanner unit, CSUX1CU (Yokogawa) and analyzed using Slide Book software. After image acquisition, the Euclidean distance of each $CD150^+$ $CD48^-$ $Lineage^-$ HSC to the closest arteriole/megakaryocyte/bone was measured in Slide Book software to generate distribution maps. For cryosections, tissues were fixed with 4% PFA via perfusion, and femoral or tibial bone tissues were further fixed with 4% PFA after dissection for 30 min at 4°C. Fixed bones were then incubated in 10%, 20%, and 30% sucrose each for 1 h at 4°C for cryoprotection and embedded in 5% carboxymethyl cellulose (SECTION-LAB). Sections, 20–30 μm thick, were prepared using Kawamoto's film method (Kawamoto and Shimizu, 2000). Alexa Fluor 488-anti-GFP (Molecular Probes) was used for enhancement of the *Snai2*-YFP signal. Anti-mouse osteocalcin antibody (R21C-01A, Takara) was used to stain osteoblasts and anti-perilipin antibody (D1D8, Cell Signaling) and BODIPY 493/503 (Molecular Probes) for adipocytes.

**Micro-CT analysis—**Micro-CT analysis of mouse femurs was done as previously described with minor modifications (Hanoun et al., 2014). Bones were fixed in 4%PFA for 48 h and then kept in PBS at 4°C until scan. The bone samples were scanned using a high-resolution SkyScan micro-CT system following a standard protocol. Images were acquired using a 10 MP digital detector, 10W power energy (100 kV and 100 μA) and a 0.5 mm aluminium filter. X-ray projections were generated from the sample obtaining both transverse and coronal slices with a 6.6 μm image pixel size. Trabecular and cortical regions

were defined as positions along the long axis of the femur relative to the growth plate reference (trabecular ROI: 0.215–1.94 mm and cortical ROI: 2.15–2.58 mm from growth plate). Morphometric analysis and 3D reconstruction were done using the SkyScan CT-analyzer software.

***In vivo* treatments and bone marrow transplantation—**For 5-FU challenge, a single dose (250 mg/kg body weight) of freshly made solution (12.5 mg/ml in sterile PBS) was given i.v. to each mouse under isoflurane anaesthesia. PolyI:C (Invivogen) was administered intra-peritoneally (i.p.) every other day at 5 mg/kg for 5 doses for *Mx1*-Cre induction. For reciprocal BM transplantation, control and Snai2CKO mice (CD45.2) were lethally irradiated (600+600 cGy, at least 3 h apart) in a Shepherd Mark-1 $^{137}$Cs irradiator and retro-orbitally injected with $1 \times 10^6$ RBC-lysed WT bone marrow nucleated cells (CD45.1) under isoflurane anaesthesia. Similarly, irradiated C57Bl/6 mice were transplanted with $1 \times 10^6$ C57Bl/6 BM cells (CD45.2) at the same time to provide competitor BM cells during secondary competitive bone marrow transplant (BMT) assays. For competitive BMT assays, $1 \times 10^6$ BM cells (CD45.2) from aforementioned competitor mice and equal volume of test bone marrow cells (CD45.1) were mixed before injection. For HSC transplant assays, 200 sorted HSCs (CD45.1) from reciprocally transplanted control and Snai2CKO mice were mixed with $0.4 \times 10^6$ BM cells (CD45.2) from aforementioned competitor mice before injection into lethally irradiated WT recipient mice (CD45.2).

**Homing assay—**Bone marrow nucleated cells ($5 \times 10^6$ cells) from wild type mice (CD45.1/CD45.2) were transplanted into lethally irradiated *Snai2*$^{+/+}$ and *Snai2*$^{-/-}$ recipient mice. Recipients were sacrificed at 3 h post transplantation and femurs and spleens were processed for FACS analysis.

**Targeted limb irradiation—**Animals were anesthetized by an intraperitoneal injection of ketamine/xylazine mix (80–100 mg/10 mg/kg) prior to irradiation using the Small Animal Radiation Research Platform, SARRP (XStrahl, Surrey, UK). The orthovoltage x-ray unit operates at 220 kVp and 13 mA. Prior to irradiation, a cone-beam computed tomography (CBCT) or static x-ray scan was acquired using 50 kVp and 0.7 mA tube current with Al filtration. Mice were maintained in a circular lucite jig at a source-surface distance (SSD) of 65cm for 771 seconds with whole body lead shielding (to protect the individualized compartments from unwanted irradiation) and a 7.5 mm port through which secured right limbs protruded and were irradiated to 12 Gy in a single fraction.

**RNA isolation and quantitative real time PCR—**Sorted cells were directly collected in 100 μl of lysis buffer and RNA isolation was performed using the Dynabeads® mRNA DIRECT™ Micro Kit following the manufacturer's instructions (Invitrogen). Reverse transcription was performed using the RNA to cDNA EcoDry™ Premix system (Clontech). Quantitative real-time PCR was performed as previously described using SYBR Green (Roche) on a QuantStudio 6 Flex Real-time PCR System (Applied Biosystems). The relative mRNA abundance was calculated using the ΔCt method using the expression of *Gapdh* as the internal control. Primer sequences can be found in the Key Resource Table.

**RNA-seq analysis—**Total RNA from 2,000-sorted CD45$^-$ Ter119$^-$ CD31$^-$ *Nes*-GFP$^+$ BM MSPCs was extracted using the RNAeasy Plus Micro kit (Qiagen), and assessed for integrity and purity using an Aligent 2100 Bioanalyzer (Agilent Technologies). Complementary DNA libraries were then generated using the SMART-Seq v4 Ultra Low Input RNA Kit for Sequencing (Clontech Laboratories) and the Nextera XT DNA Sample preparation Kit (Illumina). The libraries were then submitted for Illumina HiSeq 2500 sequencing (150bp single ended) at the Single Cell Genomics and Epigenomics Core facility at Albert Einstein College of Medicine according to the standard procedures. RNA-Seq data were then processed using a publicly available pipeline. Briefly, single-ended sequencing reads were aligned to the mouse genome (mm10) and quantified using htseq-count. Next, we normalized for RNA composition by calculating scaling factors for each sample using calcNormFactors in edgeR (version 3.12.0). Nominal p-values were corrected using the Benjamini–Hochberg procedure to adjust for multiple hypothesis testing. Differentially expressed gene sets were then identified using Ingenuity Pathways Analysis (GIAGEN Bioinformatics) and Gene Set Enrichment Analysis (GSEA) software (Broad Institute). Raw and processed reads data from the RNA-seq have been deposited in the Gene Expression Omnibus under accession number GSE142705.

### QUANTIFICATION AND STATISTICAL ANALYSIS

In each experiment, each mouse was analyzed as a biological replicate. Data in all figures were obtained in at least two independent experiments. No statistical method was used to predetermine the sample size. The experiments were not randomized and the investigators were not blinded during the experiments and outcome analyses. Data visualization and statistical analysis were performed using Graphpad Prism 7. All data are shown as mean ± s.e.m. *p< 0.05, **p< 0.01, ***p< 0.001, ****p<0.0001 by unpaired Student's *t* test unless otherwise indicated.

## Supplementary Material

Refer to Web version on PubMed Central for supplementary material.

## Acknowledgements

We thank the National Institutes of Health (DK056638, HL069438, HL116340), the Leukemia and Lymphoma Society (LLS-TRP 6475-15) and the New York State Department of Health (NYSTEM IIRP C029570 and C029154) for their support of our laboratory. We also thank Y. Zhang of the Albert Einstein College of Medicine Gene Targeting and Transgenic Core, L. Tesfa of the Flow Cytometry Sorting Facility, R. Sellers of the Histology and Comparative Pathology Facility for technical assistance and guidance, and Dr. Luis Cardoso at City College of New York for micro-CT analyses.

## References

Asada N, Kunisaki Y, Pierce H, Wang Z, Fernandez NF, Birbrair A, Ma'ayan A, and Frenette PS (2017). Differential cytokine contributions of perivascular haematopoietic stem cell niches. Nat Cell Biol 19, 214–223. [PubMed: 28218906]

Baryawno N, Przybylski D, Kowalczyk MS, Kfoury Y, Severe N, Gustafsson K, Kokkaliaris KD, Mercier F, Tabaka M, Hofree M, et al. (2019). A Cellular Taxonomy of the Bone Marrow Stroma in Homeostasis and Leukemia. Cell 177, 1915–1932 e1916. [PubMed: 31130381]

Bianco P, Cao X, Frenette PS, Mao JJ, Robey PG, Simmons PJ, and Wang CY (2013). The meaning, the sense and the significance: translating the science of mesenchymal stem cells into medicine. Nat Med 19, 35–42. [PubMed: 23296015]

Bruns I, Lucas D, Pinho S, Ahmed J, Lambert MP, Kunisaki Y, Scheiermann C, Schiff L, Poncz M, Bergman A, et al. (2014). Megakaryocytes regulate hematopoietic stem cell quiescence through CXCL4 secretion. Nat Med 20, 1315–1320. [PubMed: 25326802]

Cabezas-Wallscheid N, Klimmeck D, Hansson J, Lipka DB, Reyes A, Wang Q, Weichenhan D, Lier A, von Paleske L, Renders S, et al. (2014). Identification of regulatory networks in HSCs and their immediate progeny via integrated proteome, transcriptome, and DNA methylome analysis. Cell Stem Cell 15, 507–522. [PubMed: 25158935]

Chen Y, and Gridley T (2013). Compensatory regulation of the Snai1 and Snai2 genes during chondrogenesis. J Bone Miner Res 28, 1412–1421. [PubMed: 23322385]

Cordeiro Gomes A, Hara T, Lim VY, Herndler-Brandstetter D, Nevius E, Sugiyama T, Tani-Ichi S, Schlenner S, Richie E, Rodewald HR, et al. (2016). Hematopoietic Stem Cell Niches Produce Lineage-Instructive Signals to Control Multipotent Progenitor Differentiation. Immunity 45, 1219–1231. [PubMed: 27913094]

Denhardt DT, Noda M, O'Regan AW, Pavlin D, and Berman JS (2001). Osteopontin as a means to cope with environmental insults: regulation of inflammation, tissue remodeling, and cell survival. J Clin Invest 107, 1055–1061. [PubMed: 11342566]

Ding L, and Morrison SJ (2013). Haematopoietic stem cells and early lymphoid progenitors occupy distinct bone marrow niches. Nature 495, 231–235. [PubMed: 23434755]

Ding L, Saunders TL, Enikolopov G, and Morrison SJ (2012). Endothelial and perivascular cells maintain haematopoietic stem cells. Nature 481, 457–462. [PubMed: 22281595]

Frenette PS, Pinho S, Lucas D, and Scheiermann C (2013). Mesenchymal stem cell: keystone of the hematopoietic stem cell niche and a stepping-stone for regenerative medicine. Annu Rev Immunol 31, 285–316. [PubMed: 23298209]

Greenbaum A, Hsu YM, Day RB, Schuettpelz LG, Christopher MJ, Borgerding JN, Nagasawa T, and Link DC (2013). CXCL12 in early mesenchymal progenitors is required for haematopoietic stem-cell maintenance. Nature 495, 227–230. [PubMed: 23434756]

Guidi N, Sacma M, Standker L, Soller K, Marka G, Eiwen K, Weiss JM, Kirchhoff F, Weil T, Cancelas JA, et al. (2017). Osteopontin attenuates aging-associated phenotypes of hematopoietic stem cells. EMBO J 36, 840–853. [PubMed: 28254837]

Guo W, Keckesova Z, Donaher JL, Shibue T, Tischler V, Reinhardt F, Itzkovitz S, Noske A, Zurrer-Hardi U, Bell G, et al. (2012). Slug and Sox9 cooperatively determine the mammary stem cell state. Cell 148, 1015–1028. [PubMed: 22385965]

Hanoun M, Zhang D, Mizoguchi T, Pinho S, Pierce H, Kunisaki Y, Lacombe J, Armstrong SA, Duhrsen U, and Frenette PS (2014). Acute myelogenous leukemia-induced sympathetic neuropathy promotes malignancy in an altered hematopoietic stem cell niche. Cell Stem Cell 15, 365–375. [PubMed: 25017722]

Himburg HA, Termini CM, Schlussel L, Kan J, Li M, Zhao L, Fang T, Sasine JP, Chang VY, and Chute JP (2018). Distinct Bone Marrow Sources of Pleiotrophin Control Hematopoietic Stem Cell Maintenance and Regeneration. Cell Stem Cell 23, 370–381 e375. [PubMed: 30100167]

Inoue A, Seidel MG, Wu W, Kamizono S, Ferrando AA, Bronson RT, Iwasaki H, Akashi K, Morimoto A, Hitzler JK, et al. (2002). Slug, a highly conserved zinc finger transcriptional repressor, protects hematopoietic progenitor cells from radiation-induced apoptosis in vivo. Cancer Cell 2, 279–288. [PubMed: 12398892]

Isern J, Garcia-Garcia A, Martin AM, Arranz L, Martin-Perez D, Torroja C, Sanchez-Cabo F, and Mendez-Ferrer S (2014). The neural crest is a source of mesenchymal stem cells with specialized hematopoietic stem cell niche function. Elife 3, e03696. [PubMed: 25255216]

Jiang R, Lan Y, Norton CR, Sundberg JP, and Gridley T (1998). The Slug gene is not essential for mesoderm or neural crest development in mice. Dev Biol 198, 277–285. [PubMed: 9659933]

Kalcheim C (2015). Epithelial-Mesenchymal Transitions during Neural Crest and Somite Development. J Clin Med 5.

Kannan K, Amariglio N, Rechavi G, Jakob-Hirsch J, Kela I, Kaminski N, Getz G, Domany E, and Givol D (2001). DNA microarrays identification of primary and secondary target genes regulated by p53. Oncogene 20, 2225–2234. [PubMed: 11402317]

Kawamoto T, and Shimizu M (2000). A method for preparing 2- to 50-micron-thick fresh-frozen sections of large samples and undecalcified hard tissues. Histochem Cell Biol 113, 331–339. [PubMed: 10883392]

Kiefer FW, Zeyda M, Gollinger K, Pfau B, Neuhofer A, Weichhart T, Saemann MD, Geyeregger R, Schlederer M, Kenner L, et al. (2010). Neutralization of osteopontin inhibits obesity-induced inflammation and insulin resistance. Diabetes 59, 935–946. [PubMed: 20107108]

Kieslinger M, Hiechinger S, Dobreva G, Consalez GG, and Grosschedl R (2010). Early B cell factor 2 regulates hematopoietic stem cell homeostasis in a cell-nonautonomous manner. Cell Stem Cell 7, 496–507. [PubMed: 20887955]

Kunisaki Y, Bruns I, Scheiermann C, Ahmed J, Pinho S, Zhang D, Mizoguchi T, Wei Q, Lucas D, Ito K, et al. (2013). Arteriolar niches maintain haematopoietic stem cell quiescence. Nature 502, 637–643. [PubMed: 24107994]

Kurrey NK, Jalgaonkar SP, Joglekar AV, Ghanate AD, Chaskar PD, Doiphode RY, and Bapat SA (2009). Snail and slug mediate radioresistance and chemoresistance by antagonizing p53-mediated apoptosis and acquiring a stem-like phenotype in ovarian cancer cells. Stem Cells 27, 2059–2068. [PubMed: 19544473]

Liu X, Ma Y, Li R, Guo D, Wang N, Zhao Y, Yin J, Ren Q, Lin Y, and Ma X (2018). Niche TWIST1 is critical for maintaining normal hematopoiesis and impeding leukemia progression. Haematologica 103, 1969–1979. [PubMed: 30026340]

Mancilla A, and Mayor R (1996). Neural crest formation in Xenopus laevis: mechanisms of Xslug induction. Dev Biol 177, 580–589. [PubMed: 8806833]

Mani SA, Guo W, Liao MJ, Eaton EN, Ayyanan A, Zhou AY, Brooks M, Reinhard F, Zhang CC, Shipitsin M, et al. (2008). The epithelial-mesenchymal transition generates cells with properties of stem cells. Cell 133, 704–715. [PubMed: 18485877]

Maryanovich M, Zahalka AH, Pierce H, Pinho S, Nakahara F, Asada N, Wei Q, Wang X, Ciero P, Xu J, et al. (2018). Adrenergic nerve degeneration in bone marrow drives aging of the hematopoietic stem cell niche. Nat Med 24, 782–791. [PubMed: 29736022]

McKee MD, Farach-Carson MC, Butler WT, Hauschka PV, and Nanci A (1993). Ultrastructural immunolocalization of noncollagenous (osteopontin and osteocalcin) and plasma (albumin and alpha 2HS-glycoprotein) proteins in rat bone. J Bone Miner Res 8, 485–496. [PubMed: 8475798]

Medici D, Shore EM, Lounev VY, Kaplan FS, Kalluri R, and Olsen BR (2010). Conversion of vascular endothelial cells into multipotent stem-like cells. Nat Med 16, 1400–1406. [PubMed: 21102460]

Mendes SC, Robin C, and Dzierzak E (2005). Mesenchymal progenitor cells localize within hematopoietic sites throughout ontogeny. Development 132, 1127–1136. [PubMed: 15689383]

Mendez-Ferrer S, Michurina TV, Ferraro F, Mazloom AR, Macarthur BD, Lira SA, Scadden DT, Ma'ayan A, Enikolopov GN, and Frenette PS (2010). Mesenchymal and haematopoietic stem cells form a unique bone marrow niche. Nature 466, 829–834. [PubMed: 20703299]

Mizoguchi T, Pinho S, Ahmed J, Kunisaki Y, Hanoun M, Mendelson A, Ono N, Kronenberg HM, and Frenette PS (2014). Osterix marks distinct waves of primitive and definitive stromal progenitors during bone marrow development. Dev Cell 29, 340–349. [PubMed: 24823377]

Morikawa S, Mabuchi Y, Niibe K, Suzuki S, Nagoshi N, Sunabori T, Shimmura S, Nagai Y, Nakagawa T, Okano H, et al. (2009). Development of mesenchymal stem cells partially originate from the neural crest. Biochem Biophys Res Commun 379, 1114–1119. [PubMed: 19161980]

Nakahara F, Borger DK, Wei Q, Pinho S, Maryanovich M, Zahalka AH, Suzuki M, Cruz CD, Wang Z, Xu C, et al. (2019). Engineering a haematopoietic stem cell niche by revitalizing mesenchymal stromal cells. Nat Cell Biol 21, 560–567. [PubMed: 30988422]

Nieto MA, Sargent MG, Wilkinson DG, and Cooke J (1994). Control of cell behavior during vertebrate development by Slug, a zinc finger gene. Science 264, 835–839. [PubMed: 7513443]

Nilsson SK, Johnston HM, Whitty GA, Williams B, Webb RJ, Denhardt DT, Bertoncello I, Bendall LJ, Simmons PJ, and Haylock DN (2005). Osteopontin, a key component of the hematopoietic stem

cell niche and regulator of primitive hematopoietic progenitor cells. Blood 106, 1232–1239. [PubMed: 15845900]

Omatsu Y, Seike M, Sugiyama T, Kume T, and Nagasawa T (2014). Foxc1 is a critical regulator of haematopoietic stem/progenitor cell niche formation. Nature 508, 536–540. [PubMed: 24590069]

Park D, Spencer JA, Koh BI, Kobayashi T, Fujisaki J, Clemens TL, Lin CP, Kronenberg HM, and Scadden DT (2012). Endogenous bone marrow MSCs are dynamic, fate-restricted participants in bone maintenance and regeneration. Cell Stem Cell 10, 259–272. [PubMed: 22385654]

Perez-Losada J, Sanchez-Martin M, Perez-Caro M, Perez-Mancera PA, and Sanchez-Garcia I (2003). The radioresistance biological function of the SCF/kit signaling pathway is mediated by the zinc-finger transcription factor Slug. Oncogene 22, 4205–4211. [PubMed: 12833143]

Perez-Mancera PA, Bermejo-Rodriguez C, Gonzalez-Herrero I, Herranz M, Flores T, Jimenez R, and Sanchez-Garcia I (2007). Adipose tissue mass is modulated by SLUG (SNAI2). Hum Mol Genet 16, 2972–2986. [PubMed: 17905753]

Pinho S, Lacombe J, Hanoun M, Mizoguchi T, Bruns I, Kunisaki Y, and Frenette PS (2013). PDGFRalpha and CD51 mark human nestin+ sphere-forming mesenchymal stem cells capable of hematopoietic progenitor cell expansion. J Exp Med 210, 1351–1367. [PubMed: 23776077]

Pinho S, Marchand T, Yang E, Wei Q, Nerlov C, and Frenette PS (2018). Lineage-Biased Hematopoietic Stem Cells Are Regulated by Distinct Niches. Dev Cell 44, 634–641 e634. [PubMed: 29456137]

Seike M, Omatsu Y, Watanabe H, Kondoh G, and Nagasawa T (2018). Stem cell niche-specific Ebf3 maintains the bone marrow cavity. Genes Dev 32, 359–372. [PubMed: 29563184]

Severe N, Karabacak NM, Gustafsson K, Baryawno N, Courties G, Kfoury Y, Kokkaliaris KD, Rhee C, Lee D, Scadden EW, et al. (2019). Stress-Induced Changes in Bone Marrow Stromal Cell Populations Revealed through Single-Cell Protein Expression Mapping. Cell Stem Cell.

Stier S, Ko Y, Forkert R, Lutz C, Neuhaus T, Grunewald E, Cheng T, Dombkowski D, Calvi LM, Rittling SR, et al. (2005). Osteopontin is a hematopoietic stem cell niche component that negatively regulates stem cell pool size. J Exp Med 201, 1781–1791. [PubMed: 15928197]

Tikhonova AN, Dolgalev I, Hu H, Sivaraj KK, Hoxha E, Cuesta-Dominguez A, Pinho S, Akhmetzyanova I, Gao J, Witkowski M, et al. (2019). The bone marrow microenvironment at single-cell resolution. Nature 569, 222–228. [PubMed: 30971824]

Wei Q, Boulais PE, Zhang D, Pinho S, Tanaka M, and Frenette PS (2019). Maea expressed by macrophages, but not erythroblasts, maintains postnatal murine bone marrow erythroblastic islands. Blood 133, 1222–1232. [PubMed: 30674470]

Wu WS, Heinrichs S, Xu D, Garrison SP, Zambetti GP, Adams JM, and Look AT (2005). Slug antagonizes p53-mediated apoptosis of hematopoietic progenitors by repressing puma. Cell 123, 641–653. [PubMed: 16286009]

Yang H, Wang H, Shivalila CS, Cheng AW, Shi L, and Jaenisch R (2013). One-step generation of mice carrying reporter and conditional alleles by CRISPR/Cas-mediated genome engineering. Cell 154, 1370–1379. [PubMed: 23992847]

Zhao M, Perry JM, Marshall H, Venkatraman A, Qian P, He XC, Ahamed J, and Li L (2014). Megakaryocytes maintain homeostatic quiescence and promote post-injury regeneration of hematopoietic stem cells. Nat Med 20, 1321–1326. [PubMed: 25326798]

Zhao M, Tao F, Venkatraman A, Li Z, Smith SE, Unruh J, Chen S, Ward C, Qian P, Perry JM, et al. (2019). N-Cadherin-Expressing Bone and Marrow Stromal Progenitor Cells Maintain Reserve Hematopoietic Stem Cells. Cell Rep 26, 652–669 e656. [PubMed: 30650358]

## Highlights

- *Snai2* is required for bone marrow MSPC maintenance and regeneration.
- *Snai2* deletion compromises the HSC niche during homeostasis and after stress.
- *Snai2* suppresses osteopontin (*Spp1*) expression in MSPCs.
- Compound *Snai2* and *Spp1* knockouts rescue MSPC function.

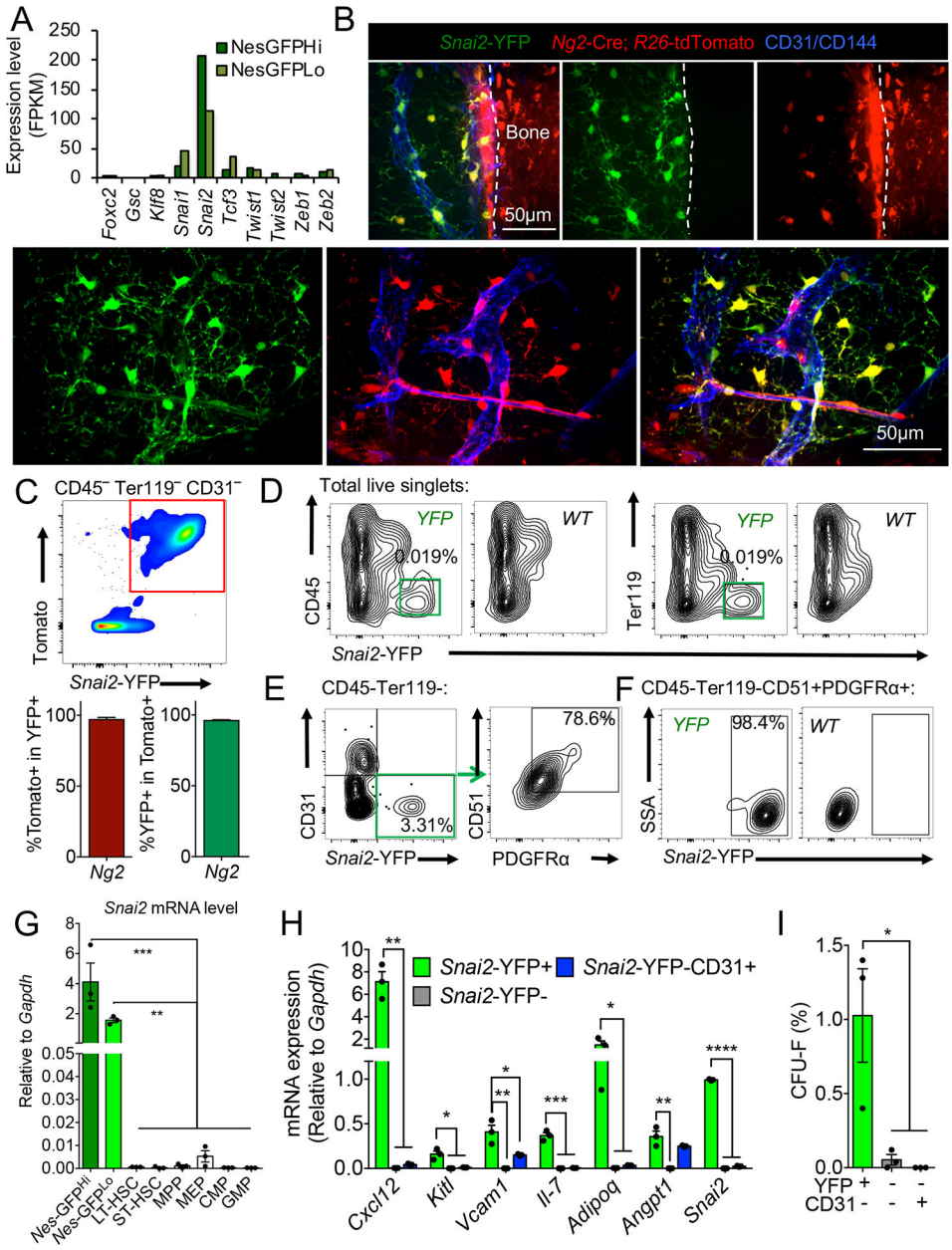


**Figure 1. *Snai2* is specifically expressed in bone marrow MSPCs.**

**(A)** Expression of EMT factors in *Nes*-GFP$^{Hi}$ and *Nes*-GFP$^{Lo}$ cells from previous RNA-seq analysis (Kunisaki et al., 2013). **(B)** Immunofluorescence images of whole-mount sterna from *Snai2*-YFP; *Ng2*-Cre; *R26*-tdTomato mice. A647-conjugated anti-CD31/CD144 antibodies were injected intravenously to label functional blood vessels. Scale bar=50μm. **(C)** FACS plot of CD45$^{-}$ Ter119$^{-}$ CD31$^{-}$ BM cells and quantifications showing nearly complete overlap between *Snai2*-YFP and *Ng2*-Cre; *R26*-tdTomato expression (n=3). **(D)** FACS plot showing restricted *Snai2*-YFP expression in the CD45$^{-}$ Ter119$^{-}$ fraction of the BM nucleated cells (BMNCs). **(E)** FACS plot showing *Snai2*-YFP labels mostly CD45$^{-}$ Ter119$^{-}$ CD31$^{-}$ CD51$^{+}$PDGFRα$^{+}$ MSPCs. **(F)** FACS plot showing that most CD45$^{-}$ Ter119$^{-}$ CD31$^{-}$ CD51$^{+}$PDGFRα$^{+}$ MSPCs are *Snai2*-YFP$^{+}$. **(G)** qRT-PCR analysis of *Snai2*

mRNA expression in sorted MSPC and hematopoietic stem and progenitor populations (*Nes*-GFP$^{hi}$ and GFP$^{lo}$: CD45$^{-}$ Ter119$^{-}$ CD31$^{-}$*Nes*-GFP$^{high}$ and GFP$^{low}$ respectively. LT-HSC: long term HSCs, ST-HSC: short term HSC, MPP: multipotent progenitors, MEP: megakaryocyte-erythrocyte progenitors, CMP: common myeloid progenitors, GMP: granulocyte-macrophage progenitors). **(H)** Niche factor mRNA levels in sorted CD45$^{-}$ Ter119$^{-}$ CD31$^{-}$ stromal populations from *Snai2*-YFP BM. **(I)** Colony forming unit-fibroblast (CFU-F) activity of sorted CD45$^{-}$ Ter119$^{-}$ CD31$^{-}$ stromal populations from *Snai2*-YFP BM.

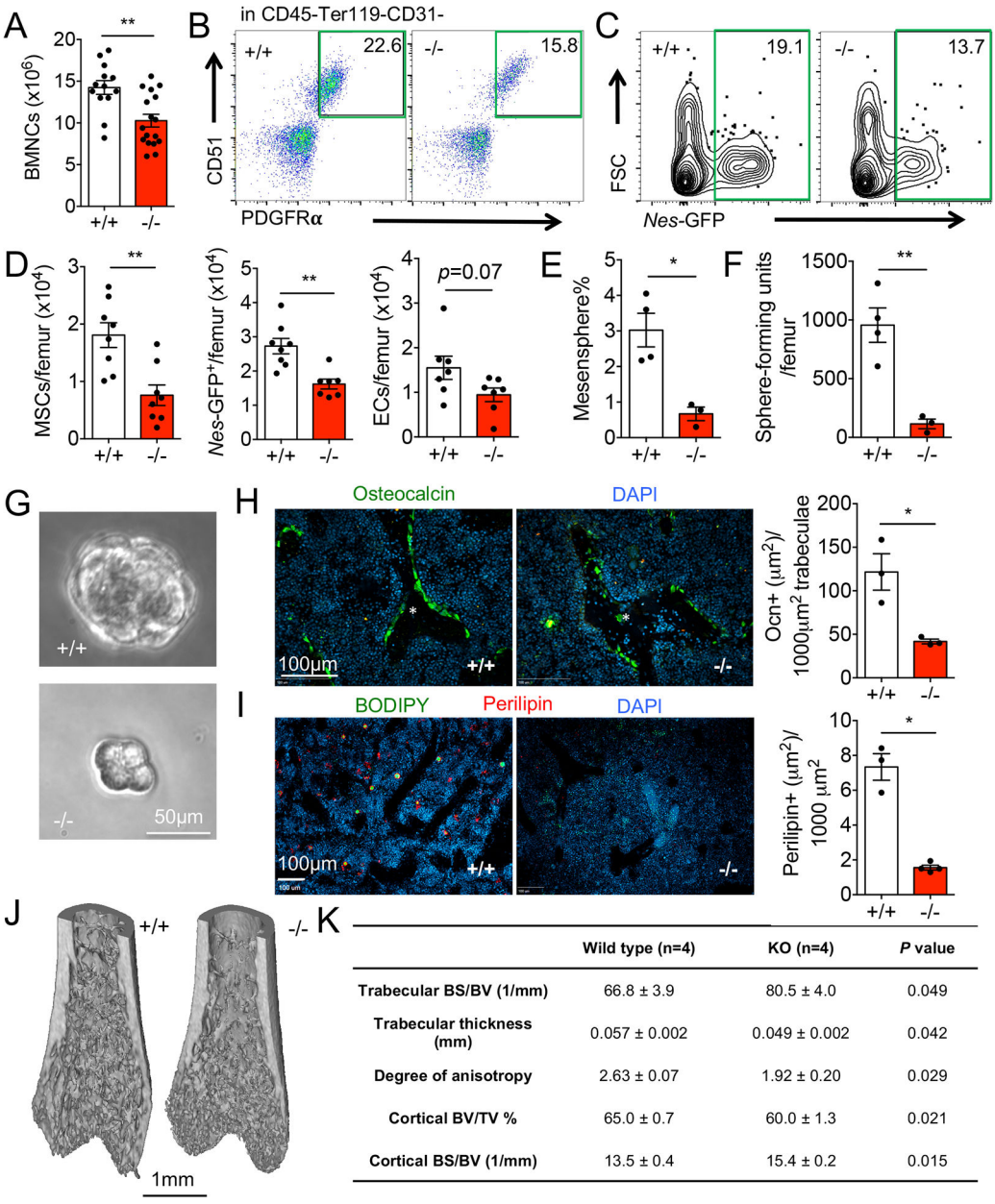


| | Wild type (n=4) | KO (n=4) | *P* value |
|---|---|---|---|
| Trabecular BS/BV (1/mm) | 66.8 ± 3.9 | 80.5 ± 4.0 | 0.049 |
| Trabecular thickness (mm) | 0.057 ± 0.002 | 0.049 ± 0.002 | 0.042 |
| Degree of anisotropy | 2.63 ± 0.07 | 1.92 ± 0.20 | 0.029 |
| Cortical BV/TV % | 65.0 ± 0.7 | 60.0 ± 1.3 | 0.021 |
| Cortical BS/BV (1/mm) | 13.5 ± 0.4 | 15.4 ± 0.2 | 0.015 |

**Figure 2. *Snai2* deletion impairs BM MSPC pool size and activity.**

**(A)** Quantification of total BMNCs from femurs of wild type (+/+) and *Snai2*-deficient (−/−) mice. **(B-D)** FACS plot of CD45$^-$ Ter119$^-$ CD31$^-$ BM cells and quantifications showing reduced CD51$^+$PDGFR$^+$ (B) and *Nes*-GFP$^+$ MSPCs (C) in the BM of *Snai2*$^{-/-}$ mice. EC, endothelial cells, defined as CD45$^-$ Ter119$^-$CD31$^+$. **(E)** Mesensphere-forming capacity of *Snai2*$^{+/+}$ and *Snai2*$^{-/-}$ BM *Nes*-GFP$^+$ MSPCs. **(F)** Sphere-forming units from femurs of *Snai2*$^{+/+}$ and *Snai2*$^{-/-}$ mice. **(G)** Bright-field images of mesenspheres formed by *Snai2*$^{+/+}$ and *Snai2*$^{-/-}$ BM *Nes*-GFP$^+$ MSPCs. **(H and I)** immunofluorescence images from frozen sections and quantifications of Osteocalcin$^+$ (Ocn$^+$) osteoblasts (H) and BODIPY$^+$ Perilipin$^+$ adipocytes (I) in control and *Snai2*$^{-/-}$ femurs. Scale bars =100μm. **(J)** Micro-CT 3D reconstruction of femurs from control and *Snai2*$^{-/-}$ mice. **(K)** Micro-CT analysis of femurs

from control and *Snai2*$^{-/-}$ mice (n=4 mice). BS, bone surface. BV, bone volume. TV, total (tissue) volume.

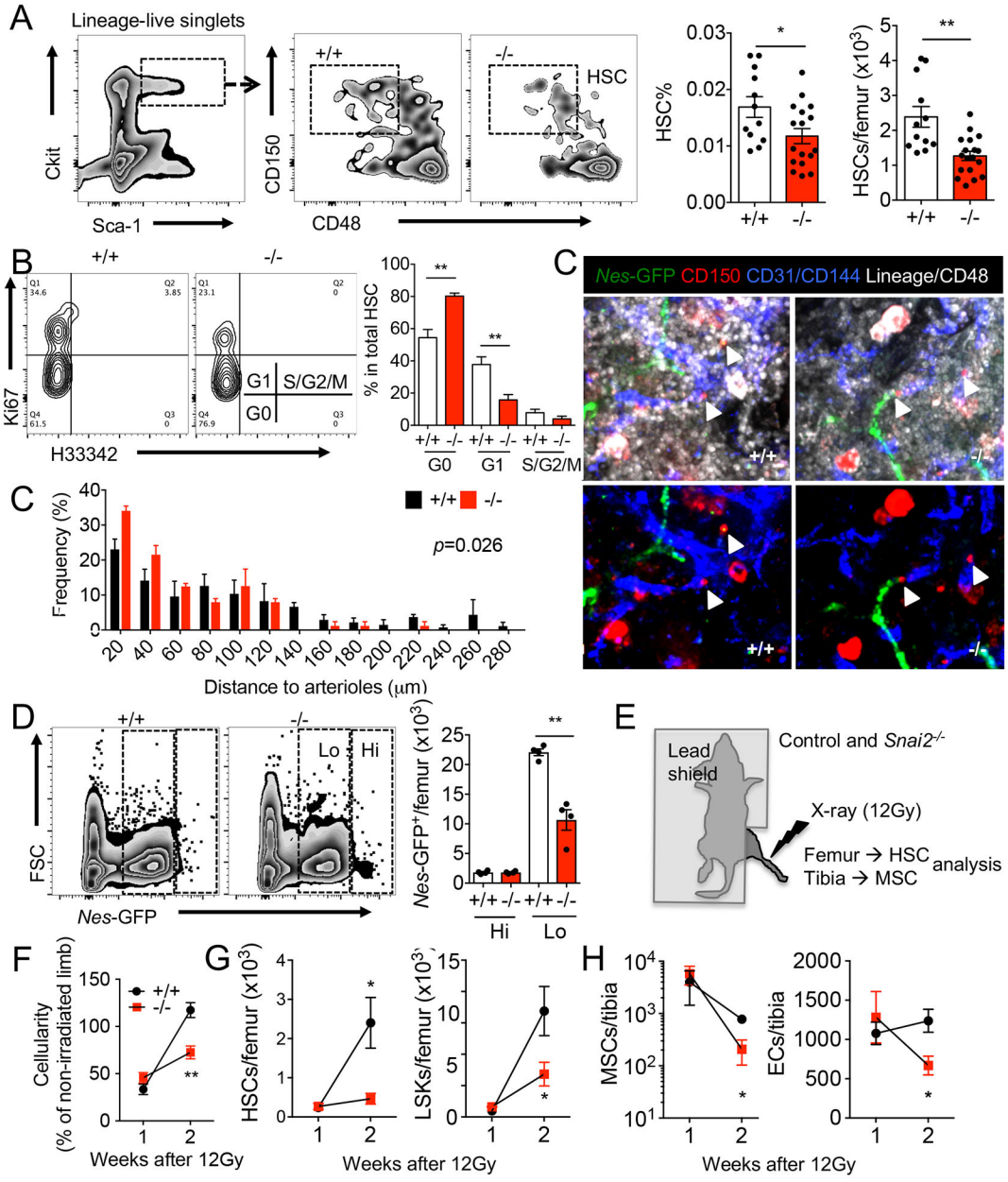


**Figure 3. *Snai2* deletion impairs BM HSC niche at steady state and after stress.**

**(A)** FACS plots and quantification of lineage$^-$ckit$^+$ Sca1$^+$ CD150$^+$ CD48$^-$ HSCs in steady state BM of *Snai2*$^{+/+}$ and *Snai2*$^{-/-}$ mice. **(B)** Cell cycle profiling of control and *Snai2*$^{-/-}$ BM HSCs by Ki-67 and H33342 staining. n=7 biological samples per group. **(C)** Whole mount immunofluorescence images of control and *Snai2*$^{-/-}$ mouse sternum and localization of HSCs (Lineage$^-$ CD48$^-$ CD150$^+$) observed *in situ* relative to *Nes*-GFP$^{Hi}$ arterioles. *p* value was determined by two-sample Kolmogorov-Smirnov test. **(D)** FACS plots and quantification of the absolute numbers of *Nes*-GFP$^{Hi}$ and *Nes*-GFP$^{Lo}$ cells in control and *Snai2*$^{-/-}$ mouse bone marrow. **(E)** Experimental design of targeted limb irradiation of control and *Snai2*$^{-/-}$ mice. **(F-H)** BM cellularity (F), HSC and LSK (lineage$^-$Sca-1$^+$Ckit$^+$)

(G) and MSPC and EC numbers (H) in irradiated legs of control and *Snai2*$^{-/-}$ mice. n=3–5 biological samples per group.

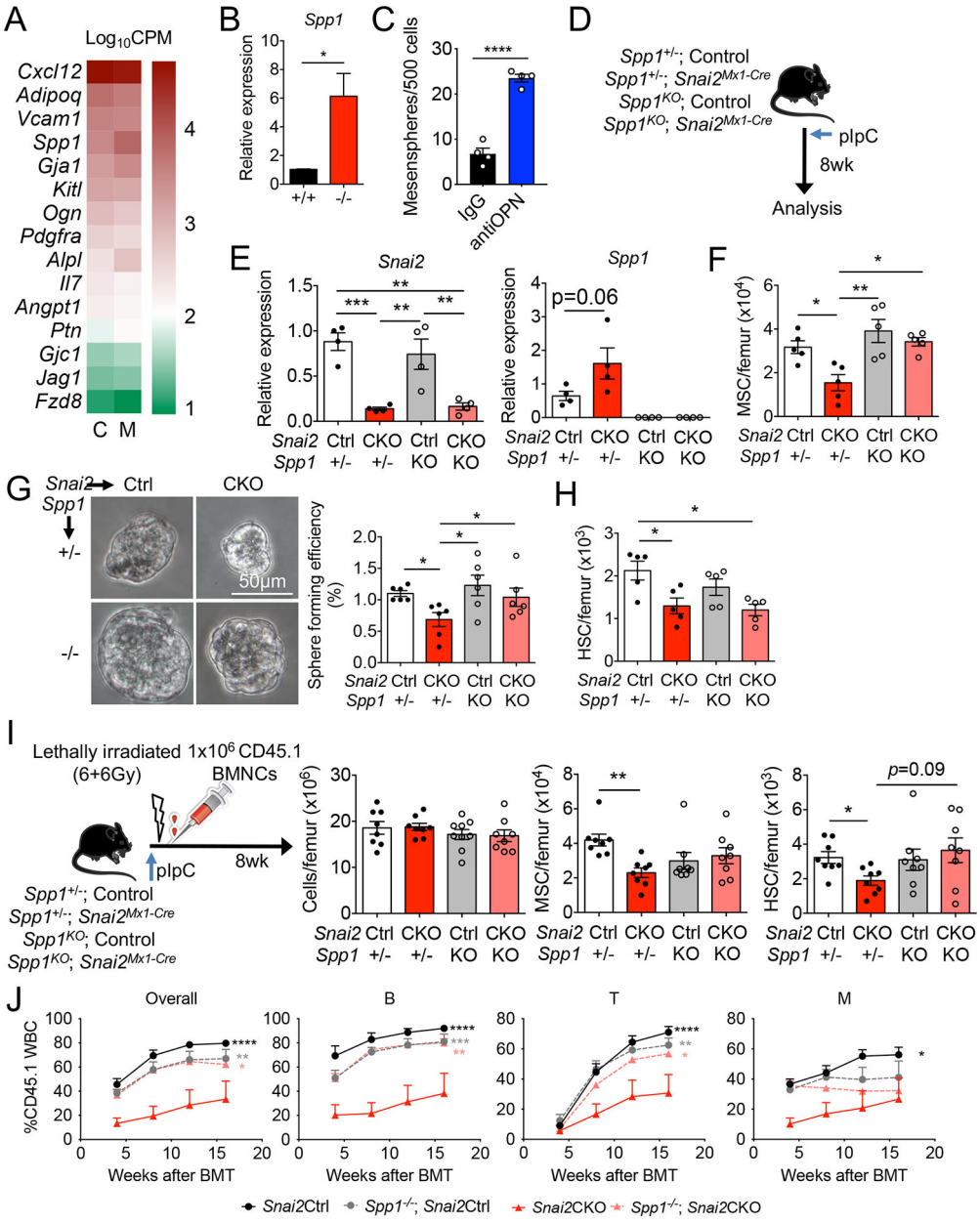


**Figure 4. *Snai2* regulates adult BM MSPC via suppression of *Spp1*.**

**(A)** RNA-seq analysis of niche factor gene expression in control (C) and *Snai2*$^{-/-}$ (M) *Nes*-GFP$^{+}$ MSPCs. n=3 per group. Gene expression levels are shown as $Log_{10}$CPM (counts per million). **(B)** qRT-PCR analysis of *Spp1* mRNA in sorted *Nes*-GFP$^{+}$ MSPC from control and *Snai2*$^{-/-}$ femurs. n=4 per group. **(C)** Mesensphere formation assay using sorted wild-type BM *Nes*-GFP$^{+}$ MSPCs in the presence of 10μg/ml anti-OPN or goat IgG. n=4 biological samples per group from two independent experiments. **(D)** Experimental scheme of inducible deletion of *Snai2* in *Snai2*$^{Mx1\text{-}Cre}$; *Spp1*$^{-/-}$ compound knockout mice. **(E)** qRT-PCR analysis of *Snai2* and *Spp1* mRNA in sorted CD45$^{-}$ Ter119$^{-}$ CD31$^{-}$ CD51$^{+}$PDGFRα$^{+}$ MSPC from *Snai2*$^{Mx1\text{-}Cre}$; *Spp1*$^{-/-}$ knockout femurs. **(F)** MSPC numbers in *Snai2*$^{Mx1\text{-}Cre}$; *Spp1*$^{-/-}$ compound knockout mice. **(G)** Bright field images and quantification of

mesensphere forming efficiency of sorted BM MSPCs from *Snai2*$^{Mx1\text{-}Cre}$; *Spp1*$^{-/-}$ compound knockout mice. **(H)** Quantification of HSC numbers in *Snai2*$^{Mx1\text{-}Cre}$; *Spp1*$^{-/-}$ mice. **(I)** Experimental design and analysis of lethally irradiated *Snai2*$^{Mx1\text{-}Cre}$; *Spp1*$^{-/-}$ mice reciprocally transplanted with wild-type (CD45.1) BM donor cells. **(J)** Peripheral blood analysis of donor-derived leukocytes (CD45.1) in lethally irradiated recipients transplanted with equal volume of BM cells from (I) (CD45.1) and WT competitors (CD45.2). n=4 mice per group. Statistical analysis was done using multiple comparisons Two-way ANOVA and significance was shown comparing *Snai2*CKO to all the other groups.

## KEY RESOURCES TABLE

| REAGENT or RESOURCE | SOURCE | IDENTIFIER |
|---|---|---|
| Antibodies | | |
| anti-mouse CD51 PE | eBioscience | Cat# 12-0512-83 |
| anti-mouse CD140a APC | eBioscience | Cat# 17-1401-81 |
| anti-mouse Ly-6A/E (Sca1) APC | eBioscience | Cat# 17-5981-83 |
| anti-mouse Ly-6A/E (Sca1) PE-Cy7 | eBioscience | Cat# 25-5981-82 |
| anti-mouse Ly-6A/E (Sca1) Alexa Fluor 700 | eBioscience | Cat# 56-5981-82 |
| anti-mouse CD117 (c-Kit) BV 421 | Biolegend | Cat#105828 |
| anti-mouse CD117 (c-Kit) PE-Cy7 | Biolegend | Cat#105814 |
| anti-mouse CD48 biotin | eBioscience | Cat#13-0481-85 |
| anti-mouse CD48 PerCP-eFluor 710 | eBioscience | Cat#46-0481-82 |
| anti-mouse CD48 FITC | eBioscience | Cat#11-0481-82 |
| anti-mouse CD41 APC | eBioscience | Cat#17-0411-82 |
| anti-mouse CD41 FITC | eBioscience | Cat#11-0411-81 |
| anti-mouse CD45.2 PE | eBioscience | Cat#12-0454-82 |
| anti-mouse CD45.2 PerCP-Cy5.5 | eBioscience | Cat#45-0454-82 |
| anti-mouse CD45.1 FITC | eBioscience | Cat#11-0453-85 |
| anti-mouse CD45.1 APC eFluor 780 | eBioscience | Cat#47-0453-82 |
| anti-mouse CD4 PE-Cy7 | eBioscience | Cat# 25-0041-82 |
| anti-mouse CD8a PE-Cy7 | eBioscience | Cat# 25-0081-82 |
| anti-mouse B220 APC eFluor 780 | eBioscience | Cat# 47-0452-82 |
| anti-mouse CD11b Alexa Fluor 647 | Biolegend | Cat# 101218 |
| anti-mouse CD31 Alexa Fluor 647 | Biolegend | Cat# 102516 |
| anti-mouse CD144 Alexa Fluor 647 | Biolegend | Cat# 138006 |
| anti-mouse Ki-67 eFluor 660 | eBioscience | Cat# 50-5698-82 |
| anti-mouse CD34 PE | Biolegend | Cat# 119308 |
| anti-mouse FcRII/III PerCP-eFluor 710 | eBioscience | Cat# 46-0161-82 |
| anti-mouse CD150 PE | Biolegend | Cat# 115904 |
| anti-mouse Ter119 PerCP-Cy5.5 | eBioscience | Cat# 45-5921-82 |
| anti-mouse Lineage panel cocktail biotin | BD Biosciences | Cat# 559971 |
| Streptavidin APC eFluor 780 | eBioscience | Cat# 47-4317-82 |
| Streptavidin eFluor 450 | eBioscience | Cat# 48-4317-82 |
| Streptavidin BV 570 | Biolegend | Cat# 405227 |
| anti-mouse osteocalcin | Takara | Cat# R21C-01A |
| anti-perilipin | Cell Signaling | Cat# D1D8 |
| Mouse Osteopontin (OPN) Affinity Purified Polyclonal Ab | R&D Systems | Cat# AF808 |
| Chemicals, Peptides, and Recombinant Proteins | | |
| BODIPY 493/503 | Molecular Probes | Cat# D3922 |

| REAGENT or RESOURCE | SOURCE | IDENTIFIER |
|---|---|---|
| 5-Fluorouracil (5-FU) | Sigma-Aldrich | Cat# F6627 |
| PolyI:C | Invitrogen | Cat# tlrl-pic |
| DAPI (4',6-diamino-2-phenylindole) | Sigma-Aldrich | D9542 |
| Hoechst 33342 | Sigma-Aldrich | B2261 |
| Collagenase IV | Gibco | Cat# 17104-019 |
| Dispase | Gibco | Cat# 17105-041 |
| DNase I | Sigma-Aldrich | Cat# DN25 |
| MesenCult stimulatory supplement | StemCell Technologies | 05502 |
| Recombinant murine EGF | PeproTech | AF-315-09 |
| Recombinant murine Oncostatin M (OSM) | R&D Systems | 495-MO-025 |
| Recombinant human IGF-1 | R&D Systems | 291-G1-200 |
| Recombinant murine PDGF-AA | PeproTech | 315-17 |
| Recombinant human FGF-basic | R&D Systems | 233-FB-025 |
| Chick Embryo Extract, Ultrafiltrate (CEE) 20ml | USBiological | C3999 |
| Human Endothelial-SFM | Gibco | 11111-044 |
| DMEM/F12, GlutaMAX | Gibco | 10565-018 |
| Critical Commercial Assays | | |
| RNA to cDNA EcoDry™ Premix system | Clontech | 639546 |
| Dynabeads® mRNA DIRECT™ Micro Kit | Invitrogen | 61012 |
| Deposited Data | | |
| RNA-seq | GSE142705 | N/A |
| Oligonucleotides used for qRT-PCR | | |
| Gapdh-F: TGTGTCCGTCGTGGATCTGA | Eurofins Genomics | N/A |
| Gapdh-R: CCTGCTTCACCACCTTCTTGA | Eurofins Genomics | N/A |
| Snai2-F: TGGTCAAGAAACATTTCAACGCC | Eurofins Genomics | N/A |
| Snai2-R: GGTGAGGATCTCTGGTTTTGGTA | Eurofins Genomics | N/A |
| Cxcl12-F: TGCATCAGTGACGGTAAACCA | Eurofins Genomics | N/A |
| Cxcl12-R: CACAGTTTGGAGTGTTGAGGAT | Eurofins Genomics | N/A |
| Kitl-F: GAATCTCCGAAGAGGCCAGAA | Eurofins Genomics | N/A |
| Kitl-R: GCTGCAACAGGGGGTAACAT | Eurofins Genomics | N/A |
| Spp1-F: TCCCTCGATGTCATCCCTGTTG | Eurofins Genomics | N/A |
| Spp1-R: GGCACTCTCCTGGCTCTCTTTG | Eurofins Genomics | N/A |
| Angpt1-F: CTCGTCAGACATTCATCATCCAG | Eurofins Genomics | N/A |
| Angpt1-R: CACCTTCTTTAGTGCAAAGGCT | Eurofins Genomics | N/A |
| Il7-F: TTCCTCCACTGATCCTTGTTCT | Eurofins Genomics | N/A |
| Il7-R: AGCAGCTTCCTTTGTATCATCAC | Eurofins Genomics | N/A |
| Vcam1-F: GACCTGTTCCAGCGAGGGTCTA | Eurofins Genomics | N/A |
| Vcam1-R: CTTCCATCCTCATAGCAATTAAGGTG | Eurofins Genomics | N/A |
| Runx2-F: TTACCTACACCCCGCCAGTC | Eurofins Genomics | N/A |

| REAGENT or RESOURCE | SOURCE | IDENTIFIER |
|---|---|---|
| Runx2-R: TGCTGGTCTGGAAGGGTCC | Eurofins Genomics | N/A |
| Cdkn1a-F: CGAGAACGGTGGAACTTTGAC | Eurofins Genomics | N/A |
| Cdkn1a-R: CAGGGCTCAGGTAGACCTTG | Eurofins Genomics | N/A |
| Bbc3-F: CTACCTCTGCGCCCCCAC | Eurofins Genomics | N/A |
| Bbc3-R: CGACTCTAAGTGCTGCTGGG | Eurofins Genomics | N/A |
| Trp53-F: GCGTAAACGCTTCGAGATGTT | Eurofins Genomics | N/A |
| Trp53-R: TTTTTATGGCGGGAAGTAGACTG | Eurofins Genomics | N/A |
| Foxc1-F: CACTCGGTGCGGGAAATGT | Eurofins Genomics | N/A |
| Foxc1-R: GGTACAGAGACTGACTGGCA | Eurofins Genomics | N/A |
| Experimental Models: Organisms/Strains | | |
| C57BL/6-*Gt(ROSA)26Sor*$^{tm1(HBEGF)Awai}$/J | The Jackson Laboratory | RRID:IMSR_JAX:007900 |
| B6; FVB-Tg(Cspg4-cre)1Akik/J | The Jackson Laboratory | RRID:IMSR_JAX:008538 |
| B6.129-Leprtm2(cre)Rck/J | The Jackson Laboratory | RRID:MGI: 3776164 |
| B6.Cg-Tg(Mx1-cre)1Cgn/J | The Jackson Laboratory | RRID:IMSR_JAX:003556 |
| Spp1Tm1Blh/J | The Jackson Laboratory | JAX: 004936 |
| C57BL/6 (CD45.2) | National Cancer Institute | |
| Bl6-Ly5.1 (CD45.1) | The Jackson Laboratory | JAX: 002014 |
| Software and Algorithms | | |
| SlideBook | Intelligent Imaging Innovations | RRID:SCR_014300 |
| FlowJo | Tree Star | RRID:SCR_008520 |
| FACS Diva 6.1 | BD Biosciences | RRID:SCR_001456 |
| Gene Set Enrichment Analysis | Broad Institute | RRID:SCR_003199 |
| Ingenuity Pathway Analysis | QIAGEN | RRID:SCR_008653 |
| GraphPad Prism | GraphPad Software | RRID:SCR_002798 |